Surfactin stimulated by pectin molecular patterns and root exudates acts as a key driver of *Bacillus*-plant mutualistic interaction

Grégory Hoff[1#], Anthony Arguelles-Arias[1], Farah Boubsi[1], Jelena Prsic[1], Thibault Meyer[1*], Heba M. M. Ibrahim[2], Sebastien Steels[1], Patricio Luzuriaga[1], Aurélien Legras[1], Laurent Franzil[1], Michelle Lequart[3], Catherine Rayon[3], Victoria Osorio[4], Edwin de Pauw[4], Yannick Lara[5], Estelle Deboever[6], Barbara de Coninck[2], Philippe Jacques[1], Magali Deleu[6], Emmanuel Petit[3], Olivier Van Wuytswinkel[3], Marc Ongena[1]

[1] Microbial Processes and Interactions, TERRA Teaching and Research Center, BioEcoAgro, Joint Research Unit/UMR transfrontalière 1158, University of Liège - Gembloux Agro-Bio Tech, Gembloux, Belgium

[2] Division of Plant Biotechnics, Department of Biosystems, Faculty of Bioscience Engineering, KU Leuven, Leuven, Belgium

[3] Unité Biologie des Plantes et Innovation, BioEcoAgro, Joint Research Unit/UMR transfrontalière 1158, Université de Picardie Jules Verne, UFR des Sciences, Amiens, France

[4] Mass Spectrometry Laboratory, MolSys Research Unit, Department of Chemistry, University of Liège, Liège, Belgium

[5] Astrobiology, UR-ASTROBIOLOGY, Geology Department, University of Liège, Liège, Belgium

[6] Molecular Biophysics at Interfaces Laboratory, Gembloux Agro-Bio Tech, University of Liège, Gembloux, Belgium

Corresponding authors: Grégory Hoff g.hoff@uu.nl
Marc Ongena marc.ongena@uliege.be

Current address: Ecology and Biodiversity, Department of Biology, Utrecht University, Padualaan 8, 3584 CH, Utrecht, The Netherlands

* Current address: UMR Ecologie Microbienne, F-69622, University of Lyon, Université Claude Bernard Lyon 1, CNRS, INRAE, VetAgro Sup, Villeurbanne, France

Abstract

Bacillus velezensis is considered as model species belonging to the so-called *B. subtilis* complex that typically evolved to dwell in the soil rhizosphere niche and establish intimate association with plant roots. This bacterium provides protection to its natural host against diseases and represents one of the most promising biocontrol agents. However, the molecular basis of the cross-talk that this bacterium establishes with its natural host has been poorly investigated. We show here that these plant-associated bacteria have evolved some polymer-sensing system to perceive their host and that in response, they increase the production of the surfactin-type lipopeptide. Furthermore, we demonstrate that surfactin synthesis is favoured upon growth on root exudates and that this lipopeptide is a key component used by the bacterium to optimize biofilm formation, motility and early root colonization. In this specific nutritional context, the bacterium also modulates qualitatively the pattern of surfactin homologues co-produced *in planta* and mainly forms variants that are the most active at triggering plant immunity. Surfactin represents a shared good as it reinforces the defensive capacity of the host.

41 **Introduction**

42 Soil is among the richest ecosystems in terms of microbial diversity, but only a subset
43 of these microbes has evolved to efficiently establish in the competitive and nutrient-
44 enriched rhizosphere layer surrounding plant roots [1]. The rhizosphere includes plant
45 beneficial bacteria dwelling on the rhizoplane as multicellular biofilm communities, feeding
46 on exuded carbohydrates [2,3], and, in turn, contributing to host fitness via growth
47 stimulation and protection against phytopathogens [4,5]. This biocontrol activity is mediated
48 via competition for nutrients and space, direct growth inhibition of the pathogenic
49 (micro)organisms and more indirectly, by stimulating the host defensive capacity in an
50 immunization-like process which leads to induced systemic resistance (ISR, [6,7]). This ISR
51 mechanism results in enhanced defense lines and reduced disease symptoms upon
52 perception of plant beneficial microbes [6,8].

53 From an ecological viewpoint, rhizosphere establishment and persistence of these
54 beneficial bacteria rely on various traits but efficient root colonization and high
55 competitiveness toward the surrounding microbiological network are pivotal. It is
56 hypothesized that the potential to produce a wide range of chemically diverse and bioactive
57 secondary metabolites (BSMs) acting as signals and/or antimicrobials is a common key
58 feature of these beneficial bacteria [5,9,10]. Members of the *Bacillus velezensis* species are
59 considered as archetypes of plant-associated beneficial bacilli and are among the most
60 prolific BSMs producers with more than 12% of their genome devoted to the synthesis of
61 compounds contributing to both ecological competence and biocontrol activity [11–15].
62 Among their BSM arsenal, the cyclic lipopeptide surfactin, is synthesized non-ribosomally by
63 a multi-modular mega-enzyme machinery (encoded by the *srfA* operon) and is formed as a
64 mix of naturally co-produced homologues varying in the length of the fatty acid chain. This
65 multifunctional compound is of particular interest because it retains important roles in key
66 developmental processes such as bacterial motility, biofilm formation and root colonization
67 [16–18], but also because it represents the best described *Bacillus* triggers for plant immunity
68 [6,8]. The potential of surfactin to stimulate ISR has been demonstrated on various plants
69 including Solanaceae like tobacco and tomato on which it acts as main if not sole elicitor
70 formed by *B. subtilis* and *B. velezensis* species [10,19]. In support to its key role in interaction
71 with the host plant, we also previously reported that surfactin is promptly formed in the

72 course of early colonization and that its production is stimulated upon sensing root tissues
73 [20].

74 However, in contrast to the well-studied interactions between plants and microbial
75 pathogens or nitrogen-fixing bacteria [21], relatively little is known on the molecular basis of
76 cooperative interactions between plants and beneficial bacteria such as *B. velezensis*
77 [11,20,22]. More specifically, how and to what extent the expression of key bacterial BSMs may
78 be modulated by plant factors is poorly understood. A better knowledge is not only critical
79 for providing new insights in rhizosphere chemical ecology but also for optimizing the use of
80 these species as biocontrol agents, which still suffer from insufficient efficacy in practice [23].
81 Here, we investigated the molecular interaction driving the early steps of partnership
82 establishment between plant roots and *B. velezensis*. We show that cell wall pectin acts in
83 synergy with soluble root exudates as plant host cues perceived by *B. velezensis*. In
84 response, the bacterium stimulates the production of specific surfactin variants as key
85 components of its secretome to further improve the fitness of both partners *i.e.* early root
86 colonization and thus rhizosphere competence of the bacterium and priming of immunity in
87 the host plant.

88

89

Results

Pectin fragments of high polymerization degree act as host cues triggering surfactin production

We previously described that early production of surfactin (as a mix of naturally co-produced homologues varying in the length of the fatty acid chain, Fig. 1) is stimulated in contact with root tissues and several plant cell wall-associated polymers (PCWP) [20]. In this work, we further investigated this phenomenon focusing on the impact of pectin, as it represents complex sugar polymers typically found in the plant primary cell wall and particularly abundant in the middle lamella layer [24]. We first tested the effect of crude pectin extracted from tobacco root PCWP (referred as cPec, Supplementary Fig. 1 for composition and related structure). An 8-fold increase of surfactin production was detected at the early exponential growth phase (OD_{600}=0.2-0.25) in *B. velezensis* GA1 liquid cultures supplemented with cPec compared to an un-supplemented culture (Fig. 1ab). Surfactin production was also 10 times enhanced upon addition at the same concentration of pure commercially available homogalacturonan (HG) with high degree of polymerization (DP) (Supplementary Fig. 2) but low level of methyl-esterification (HGLM) according to the manufacturer (Fig. 1b). HG was tested as the most abundant pectic polysaccharide constituent, which represents 65% of crude primary cell wall pectin [24]. Production of this lipopeptide was also enhanced to a similar level upon addition of highly methylated HG (HGHM), showing that the degree of methyl-esterification of the polymer is not a major trait influencing perception by the bacterium (Supplementary Fig. 3). Altogether, this supports a key role of the pectin backbone as plant molecular pattern that is sensed by the bacterium to stimulate surfactin synthesis.

Interestingly, by screening the CAZy database [25] for genes encoding carbohydrate-active enzymes potentially involved in PCWP degradation by *B. velezensis*, two putative pectate/pectin lyases encoding genes were detected. These two genes, referred as *pelA* and *pelB* (accessions *GL331_08735* and *GL331_04125 in B. velezensis* GA1*,* respectively)*,* are highly conserved among all sequenced *Bacillus* genomes that belong to the "Operational Group *B. amyloliquefaciens*" (Supplementary table 1) [26]. *pelA* and *pelB* are readily expressed in GA1 *in vitro* and the corresponding enzymes efficiently convert HG into

120 unsaturated oligogalacturonides with consistent activity occurring at the beginning of
121 stationary phase (Supplementary Fig. 4ab). However, the bacterial perception of oligomers
122 with lower polymerization degree compared to HG is not obvious since oligogalacturonides
123 (OG) did not stimulate surfactin biosynthesis (Fig. 1b, Supplementary Fig. 5 for OG
124 characterization). Supplementation with galacturonic acid (GA) led to a reduction of
125 surfactin production at mid exponential phase (OD_{600}=0.35, Supplementary Fig. 6 for growth
126 curves, Fig. 1c). Surfactin production is thus specifically boosted upon sensing long degree of
127 polymerization (DP) polymers, but is somehow inhibited in presence of GA constituting the
128 pectin backbone. Such HG-driven surfactin stimulation also occurs in other *B. velezensis*
129 isolates tested (FZB42, QST713 and S499) and to a lower extent *B. pumilus* QST 2808. It does
130 not occur in the non-rhizosphere dwelling isolates *B. amyloliquefaciens* DSM7 or *B. subtilis*
131 ATCC 21332 (Fig. 1c) suggesting that this trait may be specific to bacilli with a plant-
132 associated lifestyle.

133 **The root nutritional context favors early surfactin production**

134 *Bacillus velezensis* quickly colonize tomato plantlets in a gnotobiotic system and
135 forms visible biofilm-like structures covering the main root and embedding lateral roots after
136 24-48h post inoculation (Fig 2a). This is correlated with consistent *srfAA* gene expression and
137 surfactin production rate in the cell population at these early times but it was maintained
138 albeit to a lower level, over the investigated timeframe of seven days (Fig. 2ab). Since
139 surfactin enhancement linked to the perception of the pectin backbone is only transient (Fig
140 1b), we hypothesized that root exudates, constantly secreted by the plant, may also
141 positively impact the synthesis of the lipopeptide. Surfactin production rate was thus
142 compared upon growth in a classical laboratory medium (LB) and in a root exudate-
143 mimicking medium (REM) reflecting the content of carbohydrates typically released by
144 tomato or tobacco roots [27]. It revealed an earlier and higher production by cells growing in
145 REM (Fig 2c). Surfactin production in REM medium is initiated earlier and is more efficient in
146 *B. velezensis* compared to other closely related but non plant-associated species such as *B.*
147 *amyloliquefaciens* or *B. subtilis* (Fig. 2d).

148 Addition of HG in REM medium compared to LB revealed a cumulative effect of this
149 PCWP and root exudates on surfactin production (Fig 3a). This could be of clear ecological

150 benefit for the bacterium since surfactin is known to favor motility of multicellular
151 communities and biofilm formation [16,28,29]. However, a recent study questioned the real
152 role of surfactin in these key functions, since it production appears as non-essential for
153 pellicle biofilm formation in *B. subtilis* NCIB 3610, suggesting a strain dependant role [30]. We
154 previously reported that motility and biofilm formation are boosted upon growth on root
155 exudates [27]. Here we show that HG supplementation also favors *B. velezensis* GA1
156 spreading on low-agar medium (Fig 3b) and early biofilm formation based on pellicle
157 development at the air-liquid interface [31] (Fig 3c). The role of surfactin in swarming, pellicle
158 formation and early root colonization was further confirmed for *B. velezensis* GA1. Indeed,
159 swarming motility on low agar plates was almost reduced to zero in a surfactin deficient
160 mutant, and the same mutant was more than 3 times less efficient to produce pellicles at
161 the air liquid interface and to promptly colonize tomato roots after 1 day post inoculation
162 when compared to the WT (Fig 3def). Collectively, these data allow correlating the positive
163 impact of PCWP on bacterial motility, biofilm formation and early root colonization through
164 an anticipated surfactin production in *B. velezensis*.

165 **Surfactin induction by PCWP is not linked to major transcriptional changes.**

166 Both HG and root exudates stimulate surfactin production in GA1. However, while no
167 activation of the *srfA* biosynthetic gene cluster was observed upon HG addition
168 (Supplementary Fig. 7), an early and high surfactin gene expression was measured in
169 *srfAp*::*gfp* cells growing in REM compared to LB medium (Fig. 4a). To unravel transcriptome
170 wide changes in GA1 associated with the perception of HG, RNA-sequencing was performed
171 on cells grown in REM with our without addition of HG and collected at various time points
172 (lag, early exponential and a mid-exponential phases). The data confirmed that HG
173 perception is not linked to an increased expression of the *srfA* operon but also revealed a
174 quite limited and transient transcriptional reprogramming with only 58 genes differentially
175 expressed over this timeframe (Supplementary table 2). Remarkably, more than 30% of
176 these genes are involved in stress response or cell wall modifications and are down
177 regulated in the presence of HG (Fig. 4b). We thus hypothesize that a long-term co-evolution
178 process may have facilitated *Bacillus* establishment on the roots by the inhibition of a costly
179 stress response after perception of HG. Addition of HG also leads to a 4.2-fold reduced
180 expression of *flgM* encoding an inhibitor of SigD, the σ factor involved in the activation of

181 motility related genes [32]. This may contribute to enhanced spreading of multicellular
182 communities in addition to the positive effect of surfactin mentioned above.

183 **Root exudates drive the bacterium to form surfactin homologues with long fatty acid chain**
184 **(LFAC) and variants enriched in valine**

185 The NRPS machinery works as an assembly line in which each module is responsible
186 for recruiting and binding a specific amino acid to the nascent peptide after a first lipo-
187 initiation step for binding the fatty acid (FA) taken up from the cellular pool (Supplementary
188 Fig. 8) [33,34]. In that way, surfactin is typically composed of saturated C_{12} to C_{19}-FA of the
189 linear, iso or anteiso type of branching [35]. Beside an increased production of surfactin, we
190 also observed an effect on the pattern of surfactin variants synthesized by *B. velezensis* in
191 the presence of artificial plant exudates, as well as in naturally produced exudates and in
192 planta upon root colonization (Supplementary Fig. 9). Indeed, UPLC-MS profiling revealed
193 that the surfactin pattern produced by GA1 in REM medium is enriched in surfactin *iso*-C_{14}
194 (*i*C_{14}) and other variants compared to LB medium (Fig. 5a). They correspond to variants of
195 the canonical structure with substitution of Leu by Val for the last residue of the cyclic
196 peptide moiety (Val_7) and, to a much lower extent, to the same substitution in position 2
197 (Val_2, Fig. 5a, see Supplementary Fig. 10). Valine is used both as precursor for the synthesis
198 of branched fatty acids with an even number of carbons, and as a building block by the NRPS
199 to form the peptide moiety. Supplementation of the medium with deuterated L-Val-d^8
200 resulted in an additional increase in the proportions of surfactin *iso*-C14 and Val_7 isoforms
201 labeled at the expected positions in the peptide and in the fatty acid tail (Supplementary Fig.
202 11). Based on these data, the higher relative proportions of *i*$C_{14}Val^7$ formed in REM, but also
203 *in planta* (Fig. 5c), most probably result from some enrichment of the intracellular pool in
204 valine upon growth in the presence of root exudates (Supplementary Discussion). Given the
205 reduced specificity of NRPS domains involved in selection and activation of leucine at
206 positions 2 and 7, the megaenzyme would preferably bind valine as it is more available in the
207 pool.

208 As already described in *B. subtilis* [36,37], the pleiotropic regulator CodY acts as
209 repressor of surfactin synthesis in *B. velezensis* GA1 as illustrated by the 1.9-fold increase in
210 production by the Δ*codY* mutant of strain GA1. Interestingly, CodY activity/*codY* expression is

211 also itself negatively impacted by high cellular concentrations in branched chain amino acids
212 [38]. Both quantitative and qualitative changes in surfactin production upon growth in
213 exudates could therefore be, at least partly, due to a lower CodY activity (Supplementary
214 Discussion). In support to the role played by this regulator, a similar impact on surfactin
215 pattern were observed by deleting *codY* in GA1 or by supplementing the culture medium of
216 the wild-type with valine (Fig. 5d).

217 **Long fatty acid chain surfactins act as key triggers of receptor-independent plant immunity**

218 Based on the potential of surfactin as host immunity elicitor [9,39], we next wanted to
219 evaluate the possible relevance of quantitative and qualitative modulation of the surfactin
220 pattern driven by the plant for its own benefit.

221 Upon application as root treatment, pure surfactin used as mixture of isoforms
222 formed in REM medium, induced systemic resistance in hydroponically-grown tobacco plants
223 providing approximatively 45-50% significant disease reduction on leaves subsequently
224 infected with the pathogen *Botrytis cinerea* (Fig. 6a). The various isoforms were then HPLC-
225 purified and tested individually revealing that only long fatty acid homologues (C_{14}/C_{15})
226 provided systemic protection to a similar level whereas short fatty acid homologues (C_{12}/C_{13})
227 were inactive (Fig. 6b). Moreover, plant immunization by surfactin is dose-dependent and
228 concentrations up to 5 µM are sufficient to significantly stimulate ISR (Fig. 6c). Interestingly,
229 such low µM concentration are actually in the range of those that could accumulate in the
230 root vicinity within a few days upon colonization by GA1 (Supplementary Fig. 12).

231 We next wanted to correlate this systemic protection induced by the lipopeptide
232 with its potential to trigger locally early immune-related events such as the extracellular
233 burst in reactive oxygen species (ROS) involved in defense and signaling in pathogen-
234 triggered immunity (PTI) [40,41]. By contrast with flagellin (epitope Flg22), one of the best
235 characterized Microbe-Associated Molecular Patterns (MAMPs) isolated from bacterial
236 pathogens, treatment with surfactin did not induced burst in apoplastic ROS in root tissues
237 (Fig. 6d). However, surfactin-mediated ROS signaling still occurs since a clear cytoplasmic
238 ROS accumulation was observed (Fig 6e). Little information is available about the spatio-
239 temporal dynamics of such ROS burst but it may originate from different organelles and has
240 been occasionally described in response to perception of biotic and abiotic stresses [42,43].

241 Using cytoplasmic ROS as marker, the same trend as for ISR tests could be observed
242 regarding the influence of the structure on the activity of surfactin since long fatty acid
243 homologues but not short ones efficiently stimulated early immune reaction (Fig 6f). This
244 means that a single additional methylene group in the fatty acid tail of the molecule (C_{14}
245 versus C_{13}) likely determines its immunization potential (Fig 6b,f). By contrast, substitution of
246 Leu^7 by a Val in the C_{14} homologue does not impact activity suggesting that the peptide
247 moiety is not essential for perception by plant cells. In addition, the µM concentrations
248 required for optimal eliciting activity of surfactin are very high compared with PAMPs active
249 in the nM range [44]. Our previous data showed that surfactin elicitation is still active after
250 treating cells with proteases or after a first application indicating that there is no saturation
251 of high-affinity but low abundance binding sites on receptors [45,46]. All this indicates that
252 surfactin is perceived by plant cells via a mechanism independent of high-affinity pattern-
253 recognition receptors (PRRs) involved in MAMP perception [40,41,44,47,48]. We therefore
254 postulated that surfactin perception relies on some interaction with the lipid phase of the
255 plant plasma membrane. Binding experiments via isothermal titration calorimetry and
256 leakage assays based on the release of fluorescent probe were performed using liposomes
257 prepared with lipids specific to plant plasma membrane (PLPC/sitosterol/glucosylCeramide).
258 It revealed that long fatty acid homologues have a higher affinity for these vesicles than the
259 short fatty acid forms and display a higher destabilizing effect on the lipid bilayer when
260 added at concentrations of 5 µM or higher (Fig. 6gh). These biophysical data thus correlated
261 well with the contrasting biological activities of longer C_{14}/C_{15} and shorter C_{12}/C_{13} surfactin
262 homologues.

263 A similar cytosolic and dose-dependent ROS signature was observed in tomato roots
264 upon surfactin treatment (Supplementary Fig. 13). According to the priming concept [49], we
265 previously showed that ISR triggered by the lipopeptide in that plant as well as in tobacco
266 and *Arabidopsis*, is not associated with a fast and strong expression of defensive
267 mechanisms before pathogen infection [20,39]. In order to verify that surfactin elicitation does
268 not cause a massive release of antimicrobials from plant tissues, tomato roots were pre-
269 treated with the lipopeptide before inoculation with *B. velezensis*. As expected, it did not
270 impacted subsequent colonization in terms of rate and dynamics compared to untreated
271 plants indicating the absence of potential adverse effects on the bacterial partner (Fig. 6i).

272

Concluding remarks

A large part of the interactions between bacteria and plants is known to be mediated by small-size secreted products [50]. However, a better understanding of the chemical cross-talk at the plant-bacteria interface and its impact on bacterial ecology, plant fitness and immune responses remains challenging. In epiphytic soil bacilli, root exudates induce expression of an array of genes involved in various functions such as chemotaxis and nutrient acquisition [51–53]. Our data further illustrate that utilization of this cocktail of molecules released by roots but also the perception of some cell wall polymers may also drive these bacteria to efficiently produce key components of the secondary metabolome and more specifically the multifunctional surfactin lipopeptide [20]. As an amphiphilic molecule and powerful biosurfactant, surfactin is presumably viewed as membrane active compound with potent antimicrobial activity. However, this lipopeptide is poorly antibacterial and antifungal [54]. In *B. velezensis*, more obvious ecological functions of this CLP are to contribute to motility, biofilm formation and roots colonization. An enhanced production upon host perception thus constitutes a major force driving successful rhizosphere establishment.

Homogalacturonan acts as a cue to enhance surfactin secretion by bacterial cells but no transcriptional induction of the corresponding biosynthesis operon was observed. Surfactin synthesis is integrated in a complex network involving several pleiotropic regulators acting directly or indirectly on the expression of the *srfA* operon [55–58]. However, we hypothesize that surfactin induction by HG may rather rely on post-transcriptional changes as reported for the effect of the DegU and YczE regulators on production of another CLP, bacillomycin D [59]. Despite the relatively close genetic proximity of the two species, our data suggest that regulation of surfactin could be slightly different in *B. velezensis* and *B. subtilis*. As it represents a key infochemical devoted to cross-talk with the host plant, surfactin regulation may have been fine-tuned in rhizosphere species to better fit with the nutritional or more broadly ecological context.

Deciphering the mechanism by which *B. velezensis* recognizes pectin and enhances surfactin production would help to identify candidate genes and pathways that are responsible for plant sensing, ensuring persistence on roots which globally remains very poorly known for beneficial rhizobacteria. We are currently investigating whether some cell

304 surface proteins may act as receptors for homogalacturonan perception and binding as
305 recently described for *Sphingomonas* sp. [60], another beneficial species living in association
306 with plants [61]. Some insights could be obtained by scrutinizing the few genes conserved in
307 *B. velezensis* but missing in non-plant-associated *B. amyloliquefaciens* strains that are not
308 responsive to pectin [62]. Interestingly, shorter fragments of HG and galacturonic acid do not
309 stimulate surfactin secretion. It is therefore tempting to hypothesize that sensing unaltered
310 polymer could indicate a healthy host suitable for bacterial colonization while the perception
311 of monomers or low DP oligomers may reflect a dead or infected plant that is unable to
312 adequately provide resources.

313 Our data illustrate for the first time that *B. velezensis* can also modulate qualitatively
314 its surfactin pattern by growing in its natural nutritional context, *i.e.* on root exudates.
315 Substitution of leucine by valine in the peptide part is not expected to impact the
316 contribution of the lipopeptide to colonization by the producing strain itself considering the
317 minor effect of these structural changes on motility and biofilm formation potential [18].
318 Small modifications in the peptide sequence may nevertheless avoid surfactin hijacking for
319 use as signal prompting heterologous biofilm formation by closely related competitor
320 species [18]. Based on our observations, the most obvious benefit of an increased proportion
321 of long fatty acid chain homologues is for the host plant since they represent the most active
322 forms for priming immunity with no impact on host fitness [20,39], by contrast with PTI [63,64].
323 As the bacterial partner does not have to face strong defensive responses from this reaction,
324 it ensures positive mutualistic co-habitation allowing establishment of populations on roots.
325 Persistence of threshold populations is necessary for consistent production of other
326 specialized secondary metabolites more directly involved in warding off both microbial
327 competitors and plant soilborne pathogens in the context of biocontrol.

328 Surfactin stimulation upon sensing host molecular patterns may thus reflect an
329 aspect of plant-*Bacillus* coevolution as it makes a shared good out of this multifunctional
330 lipopeptide. To some extent, it might represent a facet of the plant-driven selection process
331 resulting in active recruitment of this bacterium as species that provides beneficial functions.
332 Other bacterial genera such as *Pseudomonas* also prevailing in the rhizosphere microbiome
333 actively produce CLPs with similar roles as surfactin. Evaluating whether their synthesis is
334 also modulated by plant cues would conceptually allow broadening the significance of these

335 lipopeptide-mediated inter-kingdom interactions for bacterial ecology, plant health and
336 biocontrol.

337

338 ## Methods

339 **Bacterial media and growth conditions.** Cultures were performed at 26°C in root exudates
340 mimicking medium (EM)[27] or in LB medium. To test the effect of plant cell wall polymers,
341 each specific plant polysaccharide was added at a final concentration of 0.1% in the culture
342 medium. Low (HGLM, <5%) and high (HGHM, >95%) methylated homogalacturonan were
343 provided from Elicityl Oligotech whereas oligogalacturonides and D-galacturonic acid were
344 provided from Sigma.

345 **Strains construction.** All the bacteria strains used in this study are listed in Supplementary
346 table 3. All the primers used in this study are available upon request. To follow the
347 expression level of the *srf* operon in GA1, we constructed a *gfp* transcriptional fusion under
348 the control of the *srf* promoter and integrated it into the *amyE* locus. First, a GA1 *amyE*
349 amplicon containing a native *KasI* restriction site was integrated in the PGEMT easy. In
350 parallel, a *cat-gfp* cassette containing respectively (i) a chloramphenicol resistance gene (cat)
351 and (ii) a promoterless *gfpmut3.1* gene was amplified with primers containing *KasI* sites at
352 their 5' extremities using the pGFP star as a matrix [65]. The pGEMT *amyE* plasmid and the
353 *cat-gfp* amplicon were both digested by *KasI* (NEB) and the two linear fragments with
354 compatible 5' overhangs were ligated together to obtain the PGEMT *amyEup-cat-gfp-*
355 *amyEdw* plasmid. To construct the final mutation cassette, an overlap extension PCR was
356 assessed by following the method developed by Bryksin and Matsumura [66]. One first
357 fragment containing the upper *amyE* homologous region and the *cat* gene, and one second
358 fragment englobing the *gfpmut3.1* gene and the lower *amyE* homologous region were both
359 amplified using the PGEMT *amyEup-cat-gfp-amyEdw* plasmid as a matrix. A third fragment
360 was amplified using GA1 genome as matrix with chimeric primers designed to obtain a *srf*
361 promoter amplicon flanked by 20 bp connectors in 5' and 3' containing respectively
362 homologies to the upper and lower *amyE* fragments. All three fragments were joined
363 together with a second PCR race to obtain the final cassette. *B. velezensis* GA1
364 transformation was performed after modification from the protocol developped by Jarmer
365 *et al.* [67].Briefly, one colony was inoculated into LB liquid medium at 37°C (160 rpm) during
366 6h and cells were washed two times with peptone water. Until 1µg of the recombinant
367 cassette was added to the GA1 cells suspension adjusted to an OD_{600nm} of 0.01 into MMG
368 liquid medium (19 g l-1 K_2HPO_4 anhydrous; 6 g l-1 KH_2PO_4; 1 g l-1 Na_3 citrate anhydrous; 0.2

369 g l-1 $MgSO_4$ $7H_2O$; 2 g l-1 Na_2SO4; 50 µM $FeCl_3$ (sterilized by filtration at 0.22 µm); 2µM
370 $MnSO_4$; 8 g l-1 Glucose; 2 g l-1 L-glutamic acid; pH 7.0). Cells were incubated at 37°C with
371 shaking, and colonies who integrated the cassette by a double crossing over event were
372 selected on LB plate supplemented with chloramphenicol. Proper integration of the *cat-gfp*
373 locus was verified by PCR. Knock-out mutant strains were constructed by gene replacement
374 by homologous recombination. A cassette containing a chloramphenicol resistance gene
375 flanked respectively by 1 kb of the upstream region and 1 kb of the downstream region of
376 the targeted gene was constructed by a three partners overlap PCR. This recombination
377 cassette was also introduced in *B. velezensis* GA1 by inducing natural competence as
378 described above [67]. Double homologous recombination event was selected by
379 chloramphenicol resistance. Deletion was confirmed by PCR analysis with the corresponding
380 upstream and downstream primers.

381 **Fluorescence measurement.** Fluorescence accumulation was evaluated thanks to the
382 channel FL1 of a BD accuri C6 flow cytometer (Biosciences) with the following parameters:
383 20000 events, medium flow rate (35 $\mu l.min^{-1}$), FSC threshold of 20000.

384 **Genome sequencing.** GA1 genome sequence was reconstructed using a combined approach
385 of two sequencing technologies which generated short paired end reads and long reads. The
386 resulted sequences were then used for hybrid assembly. More precisely, genomic DNA was
387 extracted and purified from *B. velezensis* GA1 using the GeneJET Genomic DNA purification
388 (ThermoFisher scientific). First half of extracted DNA was sent to the GIGA sequencing
389 facility (Liège, Belgium), and use as DNA template for illumina MiSeq sequencing after being
390 prepared using nextera library kit illumina. Sequencing run generated 150 bp paired-end
391 read, which were trimmed and corrected using an in-house python script and SPAdes 3.14
392 [68] before assembly. The second half of extracted DNA was used to generate long reads with
393 a MinION Oxford nanopore plateform. DNA library was constructed using the Rapid
394 Sequencing kit (SQK-RAD0004, Oxford nanopore). Adapters were trimmed from generated
395 reads with Porechop software (https://github.com/rrwick/Porechop). Trimmed reads were
396 then filtered by size (>500) and Q-score (>10) using NanoFilt implemented in NanoPack [69].
397 Finally, hybrid assembly was performed using hybridSPAdes algorithm implemented in
398 SPAdes 3.14 [70].

399 **Transcriptome library preparation and sequencing.** RNA extraction was performed for each
400 sample using the NucleoSpin RNA kit (Macherey-Nagel). Total RNAs were quantified using
401 Nanodrop (Thermofisher). For sequencing, all samples were sent to the GIGA-genomics
402 platform in Liège. Quality was assessed using the RNA 6000 Nano Chip on a 2100 Bioanalyzer
403 (Agilent). cDNA libraries were prepared employing Universal Prokaryotic RNA-Seq,
404 Prokaryotic AnyDeplete kit (Nugen) according to the manufacturer's instructions, with .
405 cDNA libraries were quantified and normalized by using the KAPA SYBR Fast Mastermix
406 (Sigma-Aldrich) with P5-P7 Illumina primers according to the manufacturer's instructions.
407 Prepared libraries were sequenced on a NextSeq 550 device (Illumina) by using the following
408 parameters : paired end, 80 cycles read 1, 8 cycles index, 80 cycles read 2.

409 **RNA-seq data analysis.** The raw RNA-seq reads were trimmed using Trimmomatic v0.39 [71].
410 We performed quality control on the trimmed reads using FastQC v0.11.8 (Babraham
411 Bioinformatics). Trimmed reads were mapped to the GA1 reference genome (see section
412 "genome sequencing" for accession numbers) using BWA-mem v0.7.17 [72] with the
413 following settings: mem -k 50 -B 40 -v 1. At least 95.4% of reads uniquely mapped to the
414 annotated reference genome (Supplementary table 4). SAMtools v1.9 [73] was used to
415 generate the BAM files and their indices. To calculate the read counts, the python-based tool
416 HTSeq v0.9 [74] was employed with the following parameters: htseq-count -q -s no -f. The
417 Cufflinks function cuffnorm [75] was used to generate the FPKM (fragments per kilobase of
418 transcript per million mapped reads) tables using the following settings: --compatible-hits-
419 norm --library-norm-method classic-fpkm. Genes with low reads counts (<25) were removed
420 before further analysis. Differential expression analysis was conducted according to the
421 DESeq2 pipeline (10.1186/s13059-014-0550-8) with cut-off parameters of $p<0.05$ and log2-
422 fold-change > 1.5.

423 **Motility and biofilm assays.** Swarming motility assays were performed according to
424 Molinatto *et al.* 2017 [76]. Diameter of the bacterial swarming pattern was measured 48h
425 after inoculation on REM soft agar plates (0.8% agar) supplemented or not with 0.1% HGLM.
426 Quantification of total biofilm was performed by crystal violet staining. Strain of interest was
427 inoculated at a final OD_{600} of 0.1 in a 96 wells microplate containing 200 µl of REM medium
428 supplemented or not with 0.1 % HGLM. The plate was incubated at 30°C during 24h without
429 shaking. Medium and planctonic cells were discarded and wells were washed with PBS.

430 Biofilm pellicle was stained with 0.1% crystal violet during 10 min and washed with PBS. The
431 stained biofilm was dissolved with 30% acetic acid. Absorbance was measured at 595 nm.

432 **Plant growth conditions and roots colonization assays.** For sterilization, tomato seeds were
433 first immersed in a 70% ethanol solution during 2 minutes, transferred in a 20% bleach
434 solution under shaking for 20 minutes and rinsed three times with sterile water. Sterilized
435 tomato seeds were pre-germinated on solid Hoagland medium at 22°C under a 16h/8h
436 night/day cycle. After 4 days, 5µL of cultures containing the strain of interest and calibrated
437 at OD_{600}=1 were deposited on the root top. After 1 and 3 days of colonization, roots were
438 harvested, deposited separately in a peptone water solution supplemented with 0.1% of
439 Tween, and vortexed vigorously to tear off the bacterial cells from the roots. Several
440 dilutions were plated on LB media to evaluate the level of colonization. Measurements of
441 surfactin production by GA1 cells colonizing roots were performed on 1x1x0.7 cm pieces of
442 gelified medium containing roots based on the assumption that the produced lipopeptide
443 diffused to a maximal distance of 5 mm from each part of the root and is uniformly
444 distributed over the surface as we previously observed via imaging-MS [77]. A 10-fold
445 concentration factor was applied to estimate concentrations around the root surface in
446 order to take into account diffusion constraints in a solid matrix. Surfactin was quantified by
447 UPLC-MS as described below.

448 **Plant cell wall extraction.** Tobacco seeds were sterilized as described above for tomato
449 seeds and deposited on Hoagland plates at 22°C during one week for a successful
450 germination process. Each plantlet was then transferred in a seedholder filled with soft agar
451 and put in Araponics boxes containing the nutritive solution described above. Cell wall
452 extraction was performed on 6 weeks old plants grown at 22°C with a 16h/8h day-night
453 alternance. Roots were harvested, lyophilized and reduced to powder using a Retsch MM400
454 grinder. 500 mg of powder was resuspended in 40 ml of ethanol 80% at 90°C for 20 min. The
455 insoluble cell wall fraction was recovered by centrifugation and the pellet obtained was
456 washed once with water to obtain the Alcoholic Insoluble Residue (AIR) used for
457 fractionation. AIR was freeze-dried before use in fractionation protocol. Sequential
458 extraction of root cell walls was performed using a protocol derived from Carpita [78] and
459 Silva *et al.* [79]. Dry AIR was resuspended in 40 ml water and incubated at 100°C for 20 min.
460 Supernatant was recovered after centrifugation as a soluble pectic fraction (cPEC).

461 **LC-MS analyses.** Detection of metabolites and quantification was performed by LC-MS. 10 µL
462 of samples were analyzed using UPLC–MS with UPLC (Acquity H-class, Waters) coupled to a
463 single quadrupole mass spectrometer (SQD mass analyzer, Waters) using an C18 column
464 (Acquity UPLC BEH C18 2.1 mm × 50 mm, 1.7 µm). Elution was performed at 40°C with a
465 constant flow rate of 0.6 mL/min using a gradient of Acetonitrile (solvent B) and water
466 (solvent A) both acidified with 0.1% formic acid as follows: starting at 15% B during 2 min,
467 solvent B was then raised from 15% to 95% in 5 min and maintained at 95% up to 9.5 min
468 before going back to initial conditions at 9.8 min during 3 minutes before next injection if
469 needed. Compounds were detected in electrospray positive ion mode by setting SQD
470 parameters as follows: source temperature 130°C; desolvation temperature 400°C, and
471 nitrogen flow: 1000 L.h-1 with mass range from m/z 800 to 1550. Surfactins were quantified
472 based on their retention times and masses compared to commercial standards (98% purity,
473 Lipofabrik).

474 **Induction of systemic resistance and ROS measurements.** ISR assays were performed as
475 previously described [39] on 4 weeks-old tobacco plants cultivated in hydroponic conditions
476 using Hoagland solution as nutrient base. Plants were treated with pure surfactin at the root
477 level and infected on leaves by applying a spore suspension of the phytopathogen *Botrytis*
478 *cinerea* prepared as detailed previously [39]. Spreading lesions occurred starting from 48h
479 post-infection and the diameter size was measured two days later. Five plants were used per
480 treatment and experiments were repeated independently at least twice. For determination
481 of cytoplasmic ROS stimulation, fluorescent probe (DCFH-DA) was used. Plants used in this
482 experiment were grown on Hoagland medium for two weeks as described above.
483 Experiments were performed on nine samples per treatment each containing three root
484 segments (approx 100 mg FW) collected from different plants (n=9). Roots were treated with
485 50 µM DCFH-DA for 10 minutes, rinsed with PBS upon removing the probe, and finally
486 treated. All the operations were conducted in a 96-well black microplate. Fluorescence
487 measurements were performed on a Spark (Tecan) microplate reader (exc 485 nm; em =
488 535 nm) with readings every 10 minutes. Stimulation of apoplastic hydrogen peroxide
489 production in root cells was measured via chemiluminescence (ferricyanide-catalysed
490 oxidation of luminol). Means and standard deviations were calculated from measurements
491 performed on three samples per treatment, each containing three root segments

492 (approximatively 100 mg FW) collected from different plants. Extracellular ROS in tomato
493 roots was conducted according to Bisceglia *et al.* [80] with minor changes. Namely, instead of
494 leaf discs, tomato roots, three segments (approximatively 100 mg FW from the same plant)
495 per sample, were used. Plants were grown for two weeks on Hoagland medium, and
496 chemiluminescence was measured in Tecan Spark plate reader.

497 **ITC analysis.** ITC analyses were performed with a VP-ITC Microcalorimeter (Microcal). The
498 calorimeter cell (volume of 1.4565 mL) was filled with a 10 µM (below the CMC
499 concentration) surfactin solution in buffer (Tris 10mM, NaCl 150mM, 1mM EDTA at pH 8.5).
500 The syringe was filled with a suspension of LUV at a lipid concentration of 5 mM. A series of
501 10µl injections was performed at constant time intervals (6 min) at 25°C. The solution in the
502 titration cell was stirred at 305 RPM. Prior to each analysis, all solutions were degassed using
503 a sonicator bath. The heats of dilution of vesicles were determined by injecting vesicles in
504 buffer and subtracted from the heats determined in the experiments. Data were processed
505 by software Origin 7 (Originlab) using the cumulative model described by Heerklotz and
506 Seelig [81]. All measurements were repeated at least three times with two different vesicle
507 preparations.

508 **Leakage assays.** Membrane permeabilization was followed as described by Van Bambeke *et*
509 *al.* [82]. Release of 8-hydroxypyrene-1,3,6 trisulfonic acid (HTPS) coentrapped with and
510 quenched by p-xylene-bis-pyridinium bromide (DPX) from liposomes can be monitored by
511 the fluorescence increase upon dilution following their leakage from the vesicles. Surfactin
512 C12 or Surfactin C14 was added from a stock solution in DMSO and fluorescence intensities
513 were immediately recorded. The percentage of HPTS released was defined as [(Ft-
514 Fcontr)/(Ftot- Fcontr)] /100, where Ft is the fluorescence signal measured after 15 min in the
515 presence of Surfactin C12 or Surfactin C14, Fcontr is the fluorescence signal measured at the
516 same time for control liposomes, and Ftot is the total fluorescence signal obtained after
517 complete disruption of the liposomes by 0.05% Triton X-100. All fluorescence determinations
518 were performed at room temperature on a Perkin Elmer LS-50B Fluorescence
519 Spectrophotometer (Perkin-Elmer Ltd.) using λexc of 450 nm and a λem of 512 nm.

520 **Statistical analyses.** All statistical analyses were performed on GraphPad prism. Before each
521 statistical analysis, variance homoscedasticity was verified by using a Brown-Forsythe test.
522 ANOVA analysis was used for multiple comparison and significant differences were indicate

523 by different letters. Statistical differences between means were evaluated by two-tailed
524 Student's t-test. Number or biological replicates used for each experiment are indicated in
525 the corresponding figure legend. P-Values are indicated in the figure legends.

526

527 **Data availability**

528 The RNA-seq datasets produced for this study are deposited at https://www.ebi.ac.uk/ena/
529 under the project reference PRJEB39762. All other datasets analyzed for this study are
530 included in the supplementary files. The Genome Resulting assembly of the GA1 strain was
531 deposited in the GenBank database under the accession numbers CP046386 and CP046387.

532

Acknowledgment

This work was supported by the EU Interreg V France-Wallonie-Vlaanderen portfolio SmartBiocontrol (Bioprotect and Bioscreen projects, avec le soutien du Fonds européen de développement régional - Met steun van het Europees Fonds voor Regionale Ontwikkeling), by the PDR research project ID 26084552 from the F.R.S.-FNRS (National fund for Scientific Research in Belgium) and by the EOS project ID 30650620 from the FWO/F.R.S.-FNRS. FB is recipient of a F.R.I.A. fellowship (Formation à la Recherche dans l'Industrie et l'Agriculture) and MO is senior research associate at the F.R.S.-F.N.R.S. We are grateful to the KU Leuven HPC infrastructure and the Flemish Supercomputer Center (VSC) for providing the computational resources and services to perform the RNA-seq analysis. We gratefully acknowledge Claire Bertrand and Loïc Ongena for critically reading the manuscript.

546 **Bibliography**

547 1. Andrews, J. H. & Harris, R. F. The Ecology and Biogeography of Microorganisms on Plant
548 Surfaces. *Annu. Rev. Phytopathol.* **38**, 145–80 (2000).

549 2. Zhalnina, K. *et al.* Dynamic root exudate chemistry and microbial substrate preferences drive
550 patterns in rhizosphere microbial community assembly. *Nat. Microbiol.* **3**, 470–480 (2018).

551 3. Vieira, S. *et al.* Drivers of the composition of active rhizosphere bacterial communities in
552 temperate grasslands. *ISME J.* **14**, 463–475 (2020).

553 4. Vacheron, J. *et al.* Plant growth-promoting rhizobacteria and root system functioning. *Front.*
554 *Plant Sci.* **4**, 1–19 (2013).

555 5. Backer, R. *et al.* Plant growth-promoting rhizobacteria: Context, mechanisms of action, and
556 roadmap to commercialization of biostimulants for sustainable agriculture. *Frontiers in Plant*
557 *Science* vol. 871 (2018).

558 6. Pieterse, C. M. J. *et al.* Induced Systemic Resistance by Beneficial Microbes. *Annu. Rev.*
559 *Phytopathol.* **52**, 347–375 (2014).

560 7. Köhl, J., Kolnaar, R. & Ravensberg, W. J. Mode of action of microbial biological control agents
561 against plant diseases: Relevance beyond efficacy. *Front. Plant Sci.* **10**, 1–19 (2019).

562 8. van Loon, L. C., Bakker, P. A. H. M. & Pieterse, C. M. J. Systemic Resistance Induced By
563 Rhizosphere Bacteria. *Annu. Rev. Phytopathol.* **36**, 453–483 (1998).

564 9. Ongena, M. *et al.* Surfactin and fengycin lipopeptides of *Bacillus subtilis* as elicitors of induced
565 systemic resistance in plants. *Environ. Microbiol.* **9**, 1084–1090 (2007).

566 10. Ongena, M. & Jacques, P. *Bacillus* lipopeptides: versatile weapons for plant disease biocontrol.
567 *Trends Microbiol.* **16**, 115–125 (2008).

568 11. Wu, K. *et al.* Pectin enhances bio-control efficacy by inducing colonization and secretion of
569 secondary metabolites by *Bacillus amyloliquefaciens* SQY 162 in the rhizosphere of tobacco.
570 *PLoS One* **10**, 1–17 (2015).

571 12. Saxena, A. K., Kumar, M., Chakdar, H., Anuroopa, N. & Bagyaraj, D. J. *Bacillus* species in soil as
572 a natural resource for plant health and nutrition. *J. Appl. Microbiol.* **128**, 1583–1594 (2020).

573 13. Chen, X. H. *et al.* Comparative analysis of the complete genome sequence of the plant growth-
574 promoting bacterium *Bacillus amyloliquefaciens* FZB42. *Nat. Biotechnol.* **25**, 1007–1014
575 (2007).

576 14. Chen, X. H. *et al.* Genome analysis of *Bacillus amyloliquefaciens* FZB42 reveals its potential for
577 biocontrol of plant pathogens. *J. Biotechnol.* **140**, 27–37 (2009).

578 15. Molinatto, G. *et al.* Complete genome sequence of *Bacillus amyloliquefaciens subsp.*
579 *plantarum* S499, a rhizobacterium that triggers plant defences and inhibits fungal
580 phytopathogens. *J. Biotechnol.* **238**, 56–59 (2016).

581 16. van Gestel, J., Vlamakis, H. & Kolter, R. From Cell Differentiation to Cell Collectives: *Bacillus*
582 *subtilis* Uses Division of Labor to Migrate. *PLoS Biol.* **13**, 1–29 (2015).

583 17. López, D., Vlamakis, H., Losick, R. & Kolter, R. Paracrine signaling in a bacterium. *Genes Dev.*
584 **23**, 1631–1638 (2009).

585 18. Aleti, G. *et al.* Surfactin variants mediate species-specific biofilm formation and root
586 colonization in *Bacillus*. *Environ. Microbiol.* **18**, 2634–2645 (2016).

587 19. Pršić, J. & Ongena, M. Elicitors of Plant Immunity Triggered by Beneficial Bacteria. *Front. Plant*
588 *Sci.* **11**, 1–12 (2020).

589 20. Debois, D. *et al.* Plant polysaccharides initiate underground crosstalk with bacilli by inducing
590 synthesis of the immunogenic lipopeptide surfactin. *Environ. Microbiol. Rep.* **7**, 570–582
591 (2015).

592 21. Gage, D. J. Infection and Invasion of Roots by Symbiotic, Nitrogen-Fixing Rhizobia during
593 Nodulation of Temperate Legumes. *Microbiol. Mol. Biol. Rev.* **68**, 280–300 (2004).

594 22. Beauregard, P. B., Chai, Y., Vlamakis, H., Losick, R. & Kolter, R. *Bacillus subtilis* biofilm
595 induction by plant polysaccharides. *Proc. Natl. Acad. Sci. U. S. A.* **110**, E1621-30 (2013).

596 23. Fan, B. *et al. Bacillus velezensis* FZB42 in 2018: The gram-positive model strain for plant
597 growth promotion and biocontrol. *Front. Microbiol.* **9**, 1–14 (2018).

598 24. Mohnen, D. Pectin structure and biosynthesis. *Curr. Opin. Plant Biol.* **11**, 266–277 (2008).

599 25. Lombard, V., Golaconda Ramulu, H., Drula, E., Coutinho, P. M. & Henrissat, B. The
600 carbohydrate-active enzymes database (CAZy) in 2013. *Nucleic Acids Res.* **42**, 490–495 (2014).

601 26. Fan, B., Blom, J., Klenk, H. P. & Borriss, R. *Bacillus amyloliquefaciens*, *Bacillus velezensis*, and
602 *Bacillus siamensis* Form an 'Operational Group *B. amyloliquefaciens*' within the *B. subtilis*
603 species complex. *Front. Microbiol.* **8**, 22 (2017).

604 27. Nihorimbere, V. *et al.* Impact of rhizosphere factors on cyclic lipopeptide signature from the
605 plant beneficial strain *Bacillus amyloliquefaciens* S499. *FEMS Microbiol. Ecol.* **79**, 176–191
606 (2012).

607 28. Chen, Y. *et al.* Biocontrol of tomato wilt disease by *Bacillus subtilis* isolates from natural
608 environments depends on conserved genes mediating biofilm formation. *Environ. Microbiol.*
609 **15**, 848–864 (2013).

610 29. Grau, R. R. *et al.* A duo of potassium-responsive histidine kinases govern the multicellular
611 destiny of *Bacillus subtilis*. *MBio* **6**, 1–16 (2015).

612 30. Thérien, M. *et al.* Surfactin production is not essential for pellicle and root-associated biofilm
613 development of *Bacillus subtilis*. *Biofilm* **2**, 100021 (2020).

614 31. Vlamakis, H., Chai, Y., Beauregard, P., Losick, R. & Kolter, R. Sticking together: Building a
615 biofilm the *Bacillus subtilis* way. *Nat. Rev. Microbiol.* **11**, 157–168 (2013).

616 32. Caramori, T., Barillà, D., Nessi, C., Sacchi, L. & Galizzi, A. Role of FlgM in σD-dependent gene
617 expression in *Bacillus subtilis*. *J. Bacteriol.* **178**, 3113–3118 (1996).

618 33. Strieker, M., Tanović, A. & Marahiel, M. A. Nonribosomal peptide synthetases: Structures and
619 dynamics. *Curr. Opin. Struct. Biol.* **20**, 234–240 (2010).

620 34. Süssmuth, R. D. & Mainz, A. Nonribosomal Peptide Synthesis—Principles and Prospects.
621 *Angew. Chemie - Int. Ed.* **56**, 3770–3821 (2017).

622 35. Diomandé, S. E., Nguyen-The, C., Guinebretière, M. H., Broussolle, V. & Brillard, J. Role of fatty
623 acids in *Bacillus* environmental adaptation. *Front. Microbiol.* **6**, 1–20 (2015).

624 36. Serror, P. & Sonenshein, A. L. CodY is required for nutritional repression of Bacillus subtilis
625 genetic competence. *J. Bacteriol.* **178**, 5910–5915 (1996).

626 37. Dhali, D. *et al.* Genetic engineering of the branched fatty acid metabolic pathway of *Bacillus*
627 *subtilis* for the overproduction of surfactin C14 isoform. *Biotechnol. J.* **12**, 1–10 (2017).

628 38. Brinsmade, S. R., Kleijn, R. J., Sauer, U. & Sonenshein, A. L. Regulation of CodY activity through
629 modulation of intracellular branched-chain amino acid pools. *J. Bacteriol.* **192**, 6357–6368
630 (2010).

631 39. Cawoy, H. *et al.* Plant Defense Stimulation by Natural Isolates of *Bacillus* Depends on Efficient
632 Surfactin Production. *Mol. Plant-Microbe Interact.* **27**, 87–100 (2014).

633 40. Saijo, Y., Loo, E. P. iian & Yasuda, S. Pattern recognition receptors and signaling in plant–
634 microbe interactions. *Plant J.* **93**, 592–613 (2018).

635 41. Waszczak, C., Carmody, M. & Kangasjärvi, J. Reactive Oxygen Species in Plant Signaling. *Annu.*
636 *Rev. Plant Biol.* **69**, 209–236 (2018).

637 42. Mignolet-Spruyt, L. *et al.* Spreading the news: Subcellular and organellar reactive oxygen
638 species production and signalling. *J. Exp. Bot.* **67**, 3831–3844 (2016).

639 43. Ashtamker, C., Kiss, V., Sagi, M., Davydov, O. & Fluhr, R. Diverse subcellular locations of
640 cryptogein-induced reactive oxygen species production in tobacco bright yellow-2 cells. *Plant*
641 *Physiol.* **143**, 1817–1826 (2007).

642 44. Bigeard, J., Colcombet, J. & Hirt, H. Signaling mechanisms in pattern-triggered immunity (PTI).
643 *Mol. Plant* **8**, 521–539 (2015).

644 45. Jourdan, E. *et al.* Insights into the defense-related events occurring in plant cells following
645 perception of surfactin-type lipopeptide from Bacillus subtilis. *Mol. Plant-Microbe Interact.* **22**,
646 456–468 (2009).

647 46. Henry, G., Deleu, M., Jourdan, E., Thonart, P. & Ongena, M. The bacterial lipopeptide surfactin
648 targets the lipid fraction of the plant plasma membrane to trigger immune-related defence
649 responses. *Cell. Microbiol.* **13**, 1824–1837 (2011).

650 47. Zipfel, C. & Oldroyd, G. E. D. Plant signalling in symbiosis and immunity. *Nature* **543**, 328–336
651 (2017).

652 48. Schellenberger, R. *et al.* Apoplastic invasion patterns triggering plant immunity: plasma
653 membrane sensing at the frontline. *Mol. Plant Pathol.* **20**, 1602–1616 (2019).

654 49. Martinez-Medina, A. *et al.* Recognizing Plant Defense Priming. *Trends Plant Sci.* **21**, 818–822
655 (2016).

656 50. Levy, A. *et al.* Genomic features of bacterial adaptation to plants. *Nat. Genet.* **50**, 138–150
657 (2018).

658 51. Fan, B. *et al.* Transcriptomic profiling of *Bacillus amyloliquefaciens* FZB42 in response to maize
659 root exudates. *BMC Microbiol.* **12**, (2012).

660 52. Feng, H. *et al.* Identification of chemotaxis compounds in root exudates and their sensing
661 chemoreceptors in plant-growth-promoting rhizobacteria *Bacillus amyloliquefaciens* SQR9.
662 *Mol. Plant-Microbe Interact.* **31**, 995–1005 (2018).

663 53. Zhang, N. *et al.* Whole transcriptomic analysis of the plant-beneficial rhizobacterium *Bacillus*
664 *amyloliquefaciens* SQR9 during enhanced biofilm formation regulated by maize root exudates.
665 *BMC Genomics* **16**, 1–21 (2015).

666 54. Raaijmakers, J. M., de Bruijn, I., Nybroe, O. & Ongena, M. Natural functions of lipopeptides
667 from *Bacillus* and *Pseudomonas*: More than surfactants and antibiotics. *FEMS Microbiol. Rev.*

668 **34**, 1037–1062 (2010).

669 55. Hayashi, K. *et al.* The H_2O_2 Stress-Responsive Regulator PerR Positively Regulates *srfA*
670 Expression in *Bacillus subtilis.* **187**, 6659–6667 (2014).

671 56. Wolf, D. *et al.* The quorum-sensing regulator ComA from *Bacillus subtilis* activates
672 transcription using topologically distinct DNA motifs. *Nucleic Acids Res.* **44**, 2160–2172 (2015).

673 57. Mariappan, A., Makarewicz, O., Chen, X. H. & Borriss, R. Two-component response regulator
674 DegU controls the expression of bacilysin in plant-growth-promoting bacterium *Bacillus*
675 *amyloliquefaciens* FZB42. *J. Mol. Microbiol. Biotechnol.* **22**, 114–125 (2012).

676 58. Zhi, Y., Wu, Q. & Xu, Y. Genome and transcriptome analysis of surfactin biosynthesis in
677 *Bacillus amyloliquefaciens* MT45. *Sci. Rep.* **7**, 1–13 (2017).

678 59. Koumoutsi, A., Chen, X. H., Vater, J. & Borriss, R. DegU and YczE positively regulate the
679 synthesis of bacillomycin D by *Bacillus amyloliquefaciens* strain FZB42. *Appl. Environ.*
680 *Microbiol.* **73**, 6953–6964 (2007).

681 60. Konishi, H., Hio, M., Kobayashi, M., Takase, R. & Hashimoto, W. Bacterial chemotaxis towards
682 polysaccharide pectin by pectin-binding protein. *Sci. Rep.* **10**, 1–12 (2020).

683 61. Muller, D. B., Schubert, O. T., Rost, H., Aebersold, R. & Vorholt, J. A. Systems-level proteomics
684 of two ubiquitous leaf commensals reveals complementary adaptive traits for phyllosphere
685 colonization. *Mol. Cell. Proteomics* **15**, 3256–3269 (2016).

686 62. Hossain, M. J. *et al.* Deciphering the conserved genetic loci implicated in plant disease control
687 through comparative genomics of *Bacillus amyloliquefaciens subsp. plantarum. Front. Plant*
688 *Sci.* **6**, 1–14 (2015).

689 63. Birkenbihl, R. P., Liu, S. & Somssich, I. E. Transcriptional events defining plant immune
690 responses. *Curr. Opin. Plant Biol.* **38**, 1–9 (2017).

691 64. Huot, B., Yao, J., Montgomery, B. L. & He, S. Y. Growth-defense tradeoffs in plants: A
692 balancing act to optimize fitness. *Molecular Plant* (2014) doi:10.1093/mp/ssu049.

693 65. Trauth, S. & Bischofs, I. B. Ectopic integration vectors for generating fluorescent promoter
694 fusions in *Bacillus subtilis* with minimal dark noise. *PLoS One* **9**, (2014).

695 66. Bryksin, A. V. & Matsumura, I. Overlap extension PCR cloning: a simple and reliable way to
696 create recombinant plasmids. *Biotechniques* **48**, 463–465 (2010).

697 67. Jarmer, H., Berka, R., Knudsen, S. & Saxild, H. H. Transcriptome analysis documents induced
698 competence of *Bacillus subtilis* during nitrogen limiting conditions. *FEMS Microbiol. Lett.* **206**,

699 197–200 (2002).

700 68. Bankevich, A. *et al.* SPAdes: A new genome assembly algorithm and its applications to single-
701 cell sequencing. *J. Comput. Biol.* **19**, 455–477 (2012).

702 69. De Coster, W., D'Hert, S., Schultz, D. T., Cruts, M. & Van Broeckhoven, C. NanoPack:
703 Visualizing and processing long-read sequencing data. *Bioinformatics* **34**, 2666–2669 (2018).

704 70. Antipov, D., Korobeynikov, A., McLean, J. S. & Pevzner, P. A. HybridSPAdes: An algorithm for
705 hybrid assembly of short and long reads. *Bioinformatics* **32**, 1009–1015 (2016).

706 71. Bolger, A. M., Lohse, M. & Usadel, B. Trimmomatic: A flexible trimmer for Illumina sequence
707 data. *Bioinformatics* **30**, 2114–2120 (2014).

708 72. Li, H. & Durbin, R. Fast and accurate short read alignment with Burrows-Wheeler transform.
709 *Bioinformatics* **25**, 1754–1760 (2009).

710 73. Li, H. *et al.* The Sequence Alignment/Map format and SAMtools. *Bioinformatics* **25**, 2078–
711 2079 (2009).

712 74. Anders, S., Pyl, P. T. & Huber, W. HTSeq-A Python framework to work with high-throughput
713 sequencing data. *Bioinformatics* **31**, 166–169 (2015).

714 75. Trapnell, C. *et al.* Transcript assembly and abundance estimation from RNA-Seq reveals
715 thousands of new transcripts and switching among isoforms. *Nat. Biotechnol.* **28**, 511–515
716 (2011).

717 76. Molinatto, G. *et al.* Key impact of an uncommon plasmid on *Bacillus amyloliquefaciens subsp.*
718 *plantarum* S499 developmental traits and lipopeptide production. *Front. Microbiol.* **8**, 1–18
719 (2017).

720 77. Debois, D., Ongena, M., Cawoy, H. & De Pauw, E. MALDI-FTICR MS imaging as a powerful tool
721 to identify *Paenibacillus* antibiotics involved in the inhibition of plant pathogens. *J. Am. Soc.*
722 *Mass Spectrom.* **24**, 1202–1213 (2013).

723 78. Carpita, N. C. Cell wall development in maize coleoptiles. *Plant Physiol.* **76**, 205–212 (1984).

724 79. Silva, G. B. *et al.* Cell wall polysaccharides from fern leaves: Evidence for a mannan-rich Type
725 III cell wall in *Adiantum raddianum*. *Phytochemistry* **72**, 2352–2360 (2011).

726 80. Bisceglia, N., Gravino, M. & Savatin, D. Luminol-based Assay for Detection of Immunity
727 Elicitor-induced Hydrogen Peroxide Production in *Arabidopsis thaliana* Leaves. *Bio-Protocol* **5**,
728 (2015).

729 81. Heerklotz, H. & Seelig, J. Titration calorimetry of surfactant-membrane partitioning and
730 membrane solubilization. *Biochim. Biophys. Acta - Biomembr.* **1508**, 69–85 (2000).

731 82. Van Bambeke, F. *et al.* Biophysical studies and intracellular destabilization of pH-sensitive
732 liposomes. *Lipids* **35**, 213–223 (2000).

733

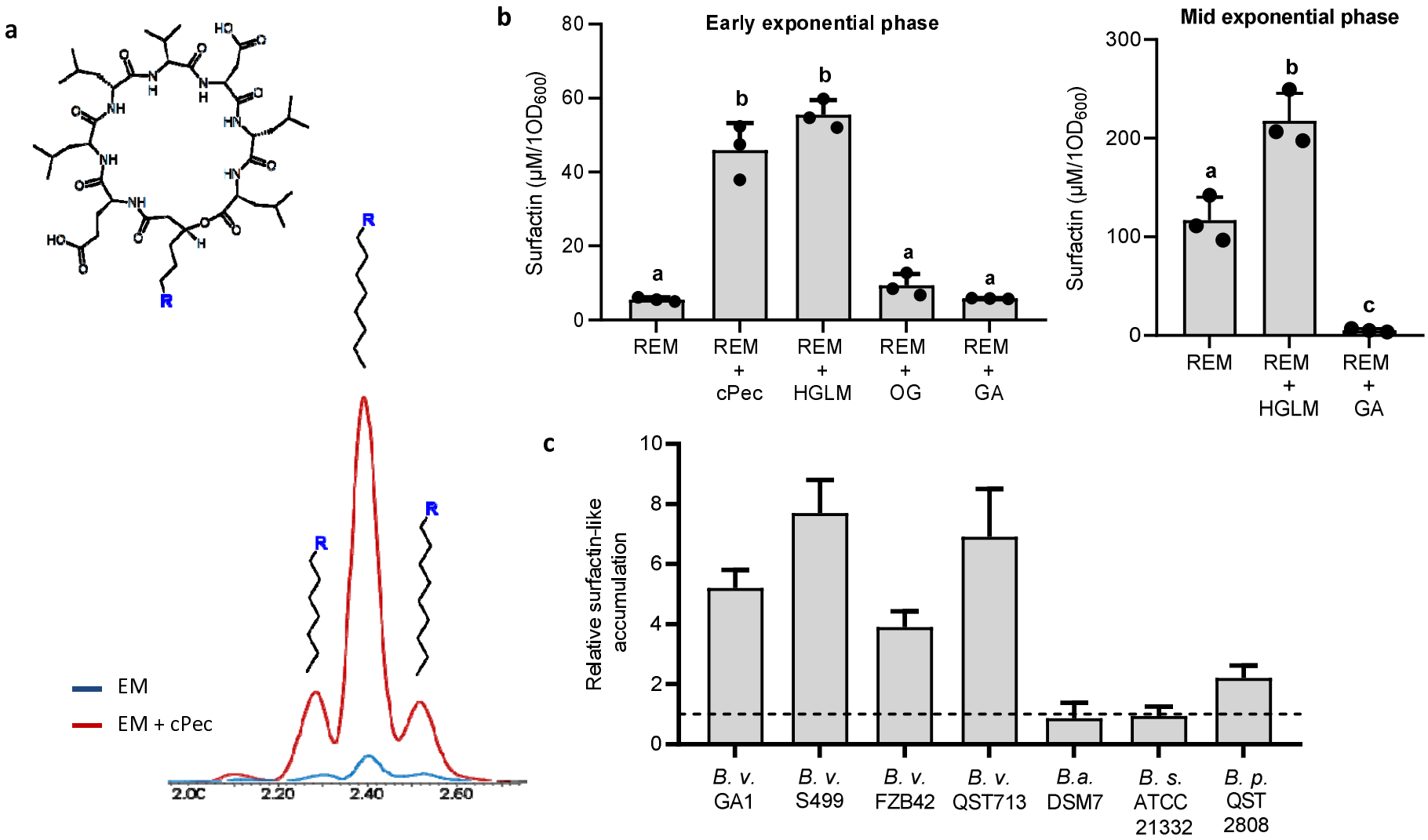
a
R
R
R
R
EM
EM + cPec
2.00
2.20
2.40
2.60
b
Early exponential phase
Surfactin (µM/1OD600)
80
60
40
20
0
a
b
b
a
a
REM
REM + cPec
REM + HGLM
REM + OG
REM + GA
Mid exponential phase
Surfactin (µM/1OD600)
300
200
100
0
a
b
c
REM
REM + HGLM
REM + GA
c
Relative surfactin-like accumulation
10
8
6
4
2
0
B. v. GA1
B. v. S499
B. v. FZB42
B. v. QST713
B.a. DSM7
B. s. ATCC 21332
B. p. QST 2808

Figure 1: Impact of pectin on early surfactin production. a Surfactin (cyclic structure represented up) production in a root exudates mimicking (REM) medium at early growth phase (OD_{600}=0.2) with (red chromatogram) or without (blue chromatogram) addition of crude pectin extract added to the GA1 cultures. The main peak represents C15 surfactin whereas the minor left and right peaks represents C14 and C16 surfactins, respectively. **b** Surfactin accumulation in the early (left panel, OD_{600}=0.2) and mid (right panel, OD_{600}=0.35) exponential growth phase of GA1 cultures in REM medium supplemented with different sized pectin fragments : homogalacturonan low methylated (HGLM), DP>150; oligogalacturonides (OG), DP=15; galacturonic acid (GA), DP=1. Means ± std err. from three biological replicates of one representative experiment are shown. Significate difference between each condition is indicated by different letters, p-value < 0.01. **c** Comparison of surfactin induction level by HGLM in the early exponential growth phase for different *Bacillus* species : *Bacillus velezensis* (*B; v*), *Bacillus amyloliquefaciens* (*B. a*), *Bacillus subtilis* (*B. s*) and *Bacillus pumilus* (*B. p*). For each strain tested, surfactin accumulation was normalized with the control condition without HGLM represented by the black dotted line. Means ± std err. from three biological replicates are shown.

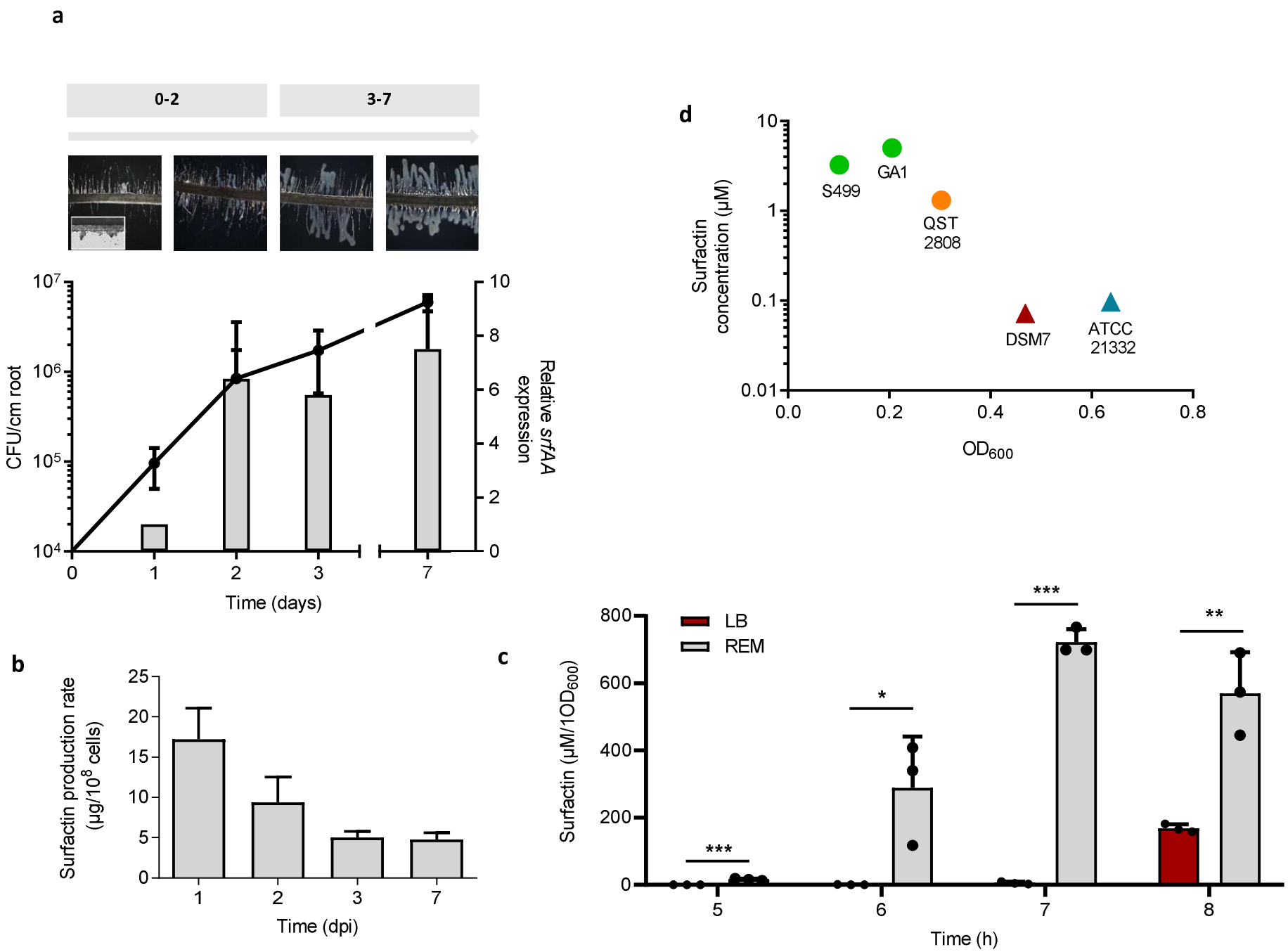
a
0-2
3-7
CFU/cm root
Relative srfAA expression
Time (days)
b
Surfactin production rate (µg/10^8 cells)
Time (dpi)
c
LB
REM
Surfactin (µM/1OD600)
Time (h)
d
Surfactin concentration (µM)
OD600
S499
GA1
QST 2808
DSM7
ATCC 21332

Figure 2: Impact of the specific rhizosphere nutritional context on early surfactin production. a Evaluation of bacterial population (black line, left axis) and relative *srfAA* expression on roots (grey bars, right axis) in a time frame of seven days post inoculation (dpi). *Bacillus* progression on roots characterized by a biofilm formation was assessed by microscopy at each time point (upper part). **b** Surfactin production rate on roots. Means ± std err. from three biological replicates of one representative experiment are shown **c** Surfactin accumulation measured by UPLC-MS in a 8h time course experiment in REM medium (grey bars) compared to LB medium (red bars). Means ± std err. from three biological replicates of one representative experiment are shown *** P-value <0.001, ** P-value <0.01, * P-value <0.05 **d** Comparison of early surfactin accumulation (µM of surfactin on y axis linked to OD_{600} on x axis) in different *Bacillus* species, including *B. velezensis* (GA1 and S499 in green), *B. pumilus* (QST 2808 in orange), *B. amyloliquefaciens* (DSM 7 in red) and *B. subtilis* (ATCC 21332 in blue). Circle symbols are representing plant associated bacteria whereas triangle symbols are representing non-plant associated bacteria.

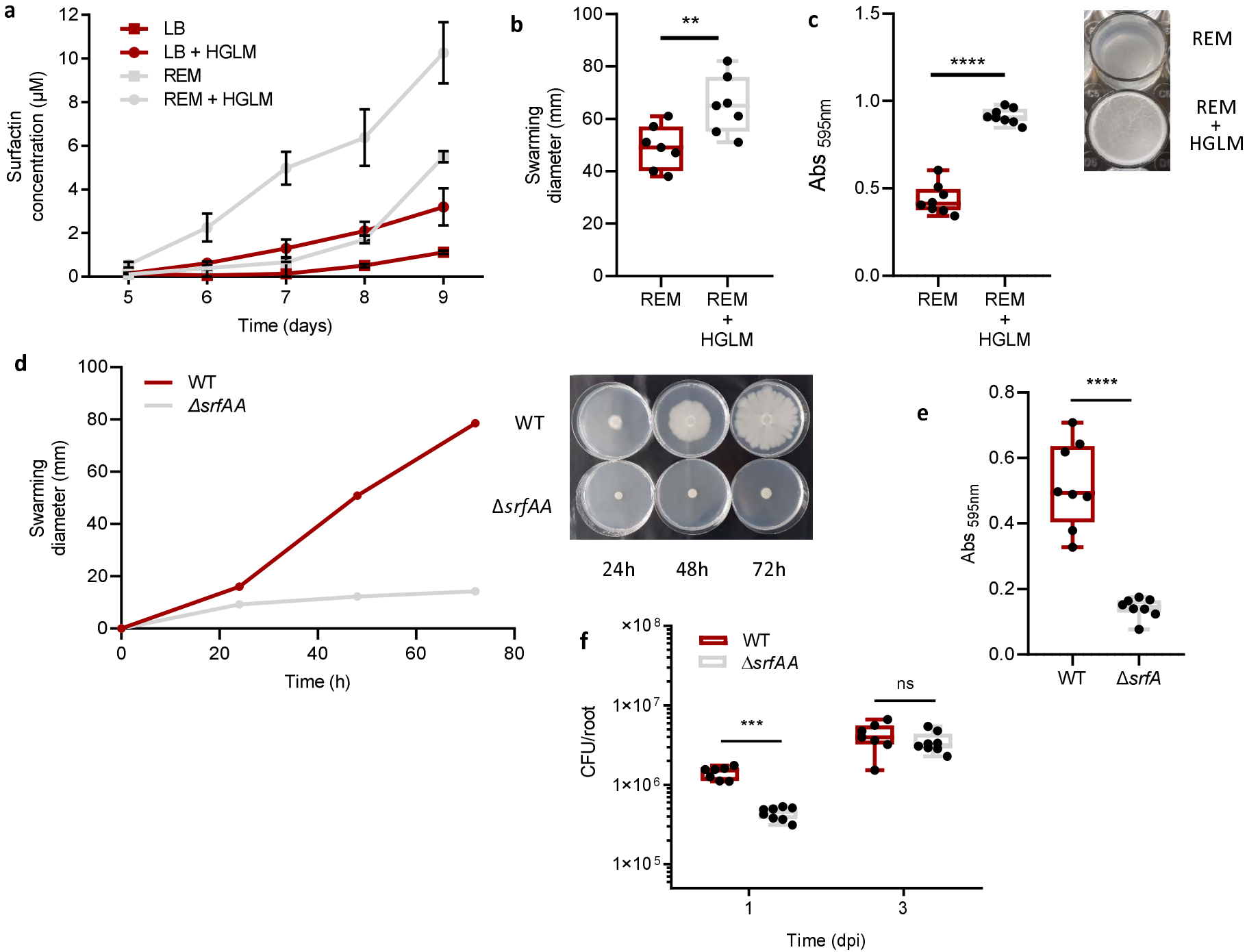
a
Surfactin concentration (µM)
Time (days)
LB
LB + HGLM
REM
REM + HGLM
b
Swarming diameter (mm)
**
REM
REM + HGLM
c
Abs 595nm
****
REM
REM + HGLM
d
Swarming diameter (mm)
Time (h)
WT
ΔsrfAA
WT
ΔsrfAA
24h
48h
72h
e
Abs 595nm
****
WT
ΔsrfA
f
CFU/root
Time (dpi)
WT
ΔsrfAA
***
ns

Figure 3: Ecological importance of an early surfactin accumulation. a Evaluation of HGLM and root exudates synergistic effect on early surfactin production. Time course experiment for surfactin quantification was performed in REM (grey curves) and LB (red curves) medium with (circle symbols) or without (square symbols) addition of HGLM. Means ± std err. from three biological replicates of one representative experiment are shown **b** Swarming potential of *B. velezensis* GA1 on soft agar plates after addition of HGLM or not. Means ± std err. from seven biological replicates of one representative experiment are shown. **c** Evaluation of *B. velezensis* ability to form pellicles on microwells plates after addition of HGLM or not. Means ± std err. from eight biological replicates of one representative experiment are shown. Pellicle formation is illustrated on the right **d** Comparison of *B. velezensis* GA1 WT and (red) and a Δ*srfAA* mutant (grey) for their swarming potential in a time course study. Means ± std err. from three biological replicates of one representative experiment are shown. Time course study is illustrated right. **e** Comparison of pellicle formation between GA1 WT strain (red) and a Δ*srfAA* mutant (grey). Means ± std err. from eight biological replicates of one representative experiment are shown **** P-value <0.0001. **f** *In vitro* comparison of root colonization ability of GA1 (red boxes) and GA1 Δ*srfAA* (grey boxes) on tomato plantlets. Means ± std err. from eight biological replicates of one representative experiment are shown *** P-value <0.001, ns non significant.

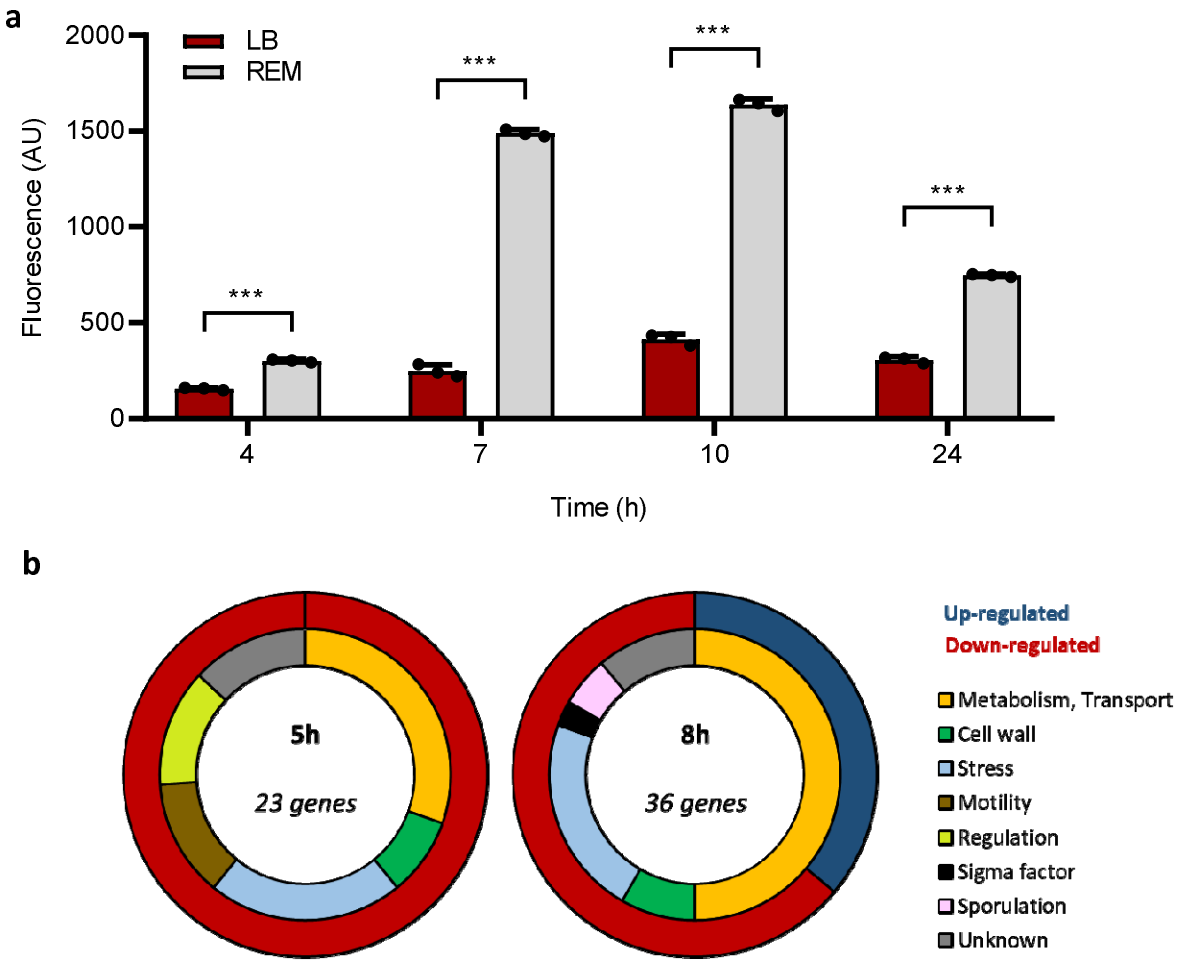

Figure 4: Impact of plant triggers perception on *Bacillus* transcriptome. a Surfactin expression measured by fluorescence in the GA1 P*srfAp::gfp* reporter strain in a 24h time course study in EM medium (grey bars) compared to LB medium (red bars). Means ± std err. from three biological replicates of one representative experiment are shown *** P-value <0.001. **b** Classification of the different genes carrying a significant fold change (1.5 log2) 5 and 8 hours after addition of HG when compared to the control condition. The outer circle represents the proportion of up (dark blue) and down (red) regulated genes. The inner circle represents the proportion of genes belonging to the different functional family described in the legend.

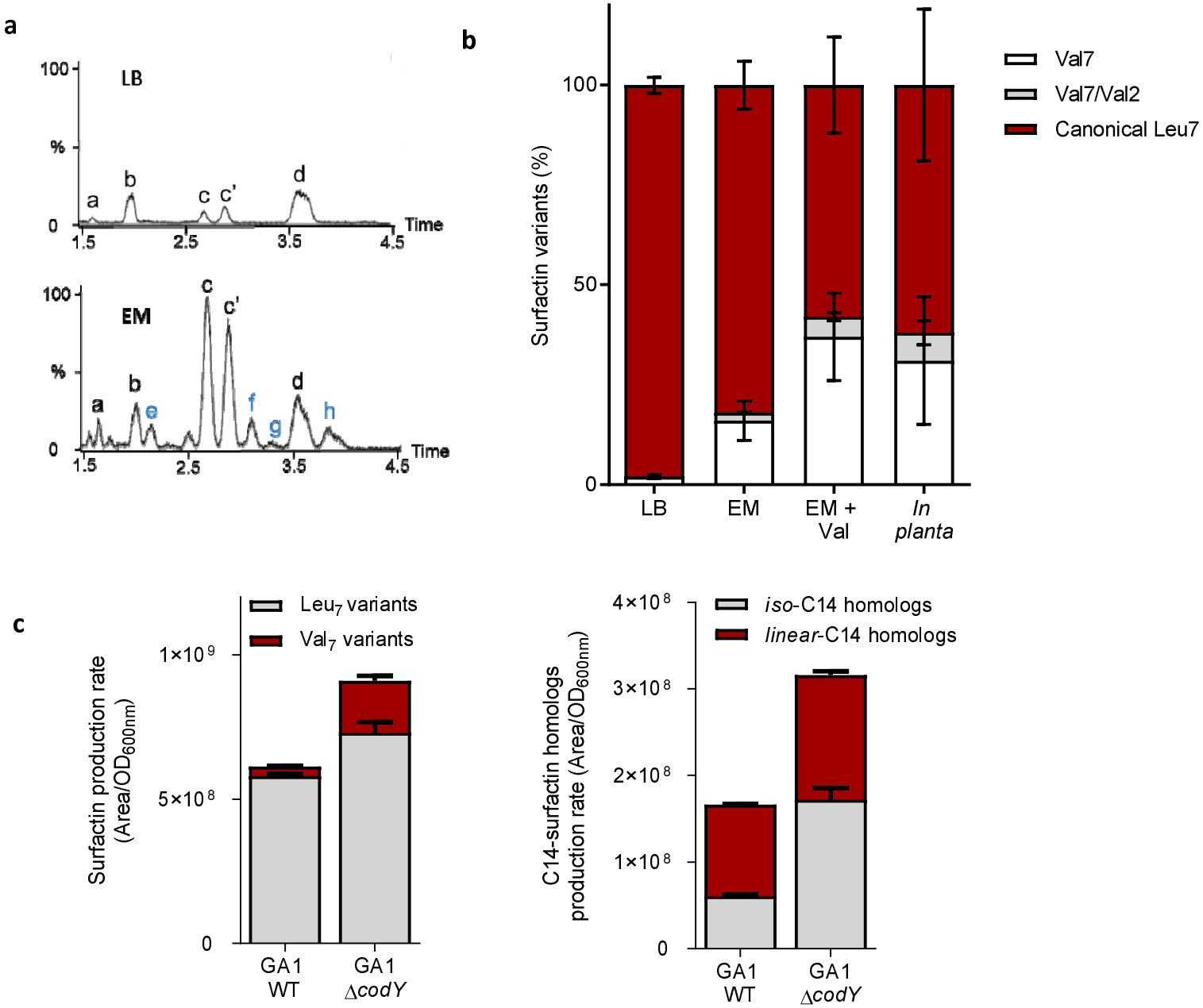
a
LB
100
%
0
a
b
c
c'
d
Time
1.5
2.5
3.5
4.5
EM
c
c'
b
e
f
g
d
h
b
Surfactin variants (%)
100
50
0
LB
EM
EM + Val
In planta
Val7
Val7/Val2
Canonical Leu7
c
Leu7 variants
Val7 variants
Surfactin production rate (Area/OD600nm)
1×10 9
5×10 8
0
GA1 WT
GA1 ΔcodY
iso-C14 homologs
linear-C14 homologs
C14-surfactin homologs production rate (Area/OD600nm)
4×10 8
3×10 8
2×10 8
1×10 8
0
GA1 WT
GA1 ΔcodY

Figure 5: Qualitative impact of root exudates on surfactin production. **a** Comparison of surfactin pattern in REM and LB medium. Based on MS-MS analyses, nine different surfactin forms were identified (a: C_{12}-Glu-Leu-Leu-Val-Asp-Leu-Leu ; b: C_{13}-Glu-Leu-Leu-Val-Asp-Leu-Leu ; c : *iso*-C_{14}-Glu-Leu-Leu-Val-Asp-Leu-Leu ; c': *n*-C_{14}-Glu-Leu-Leu-Val-Asp-Leu-Leu ; d : C_{15}-Glu-Leu-Leu-Val-Asp-Leu-Leu ; e: C_{13}-Glu-Leu-Leu-Val-Asp-Leu-Val ; f: C_{14}-Glu-Leu-Leu-Val-Asp-Leu-Val ; g: C_{14}-Glu-Leu-Leu-Val-Asp-Leu-Val and h: C_{14}-Glu-Val-Leu-Val-Asp-Leu-Val.) **b** Relative proportions of surfactin variants in LB, REM, REM supplemented with valine, and *in planta.* **c** Qualitative and quantitative role of CodY on surfactin production. In a WT strain, 95% of the surfactin molecules are carrying a Leu in position 7 (grey bars) and only 5% are carrying a Val (red bars) whereas in Δ*codY* mutant almost 25% of the surfactin molecules are carrying a Val in position 7 and 75% a Leu. In addition, amount of total surfactin production rate of 150 % can be observed in Δ*codY* mutant compared to WT strain. Proportion of iso-C14 is also affected by CodY, 36 % of total C_{14} are iso-fatty acid (grey bars) and 64% are linear (red bars) in WT strain whereas in Δ*codY* mutant 55% of C_{14} are *iso*-C_{14} and 45 % are linear. Again, total amount of C_{14} is higher in Δ*codY* mutant (increase of 190 %).

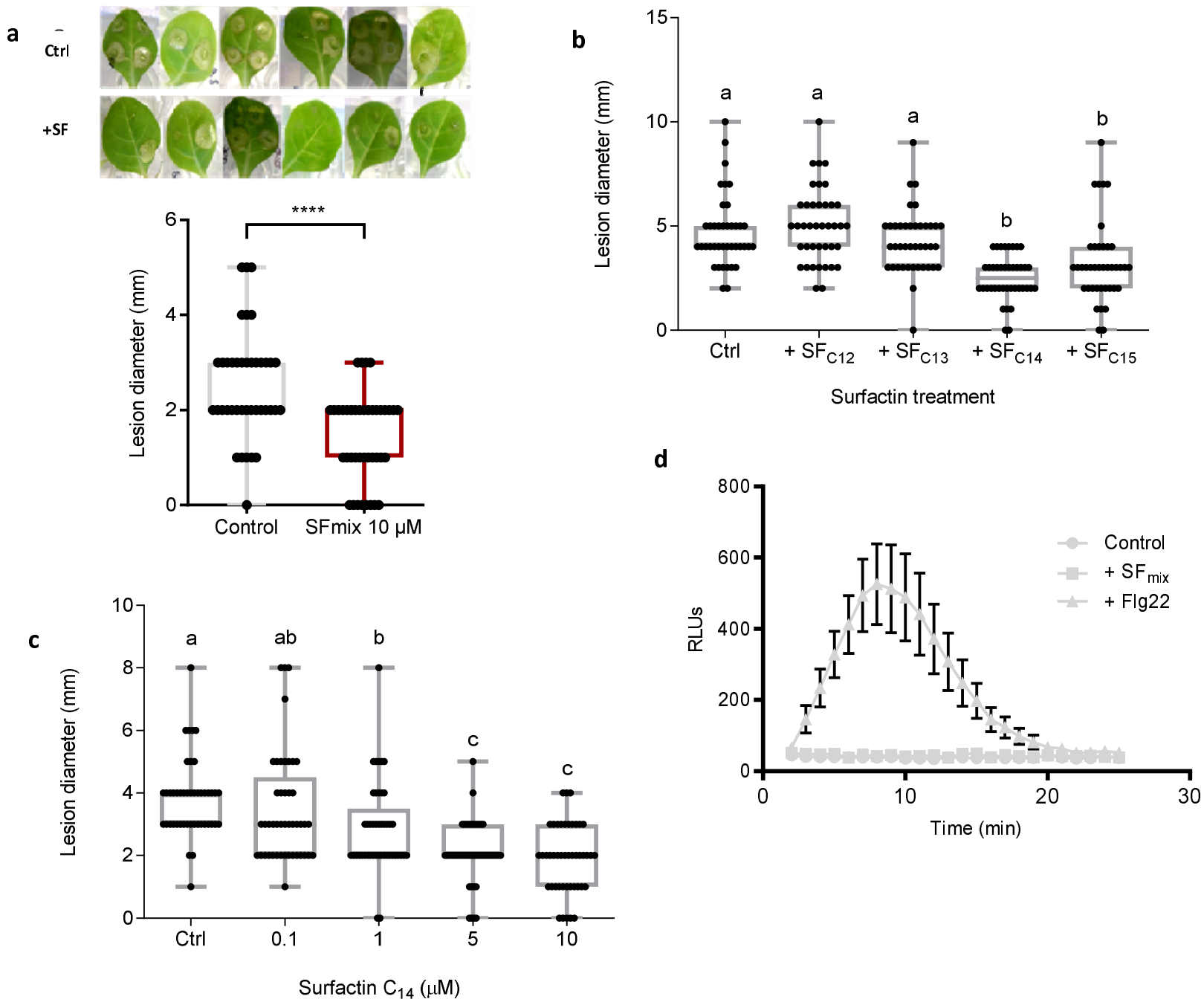
a
Ctrl
+SF
****
Lesion diameter (mm)
Control
SFmix 10 µM
b
Lesion diameter (mm)
a
a
a
b
b
Ctrl
+ SF$_{C12}$
+ SF$_{C13}$
+ SF$_{C14}$
+ SF$_{C15}$
Surfactin treatment
c
Lesion diameter (mm)
a
ab
b
c
c
Ctrl
0.1
1
5
10
Surfactin C$_{14}$ (µM)
d
RLUs
Control
+ SF$_{mix}$
+ Flg22
Time (min)

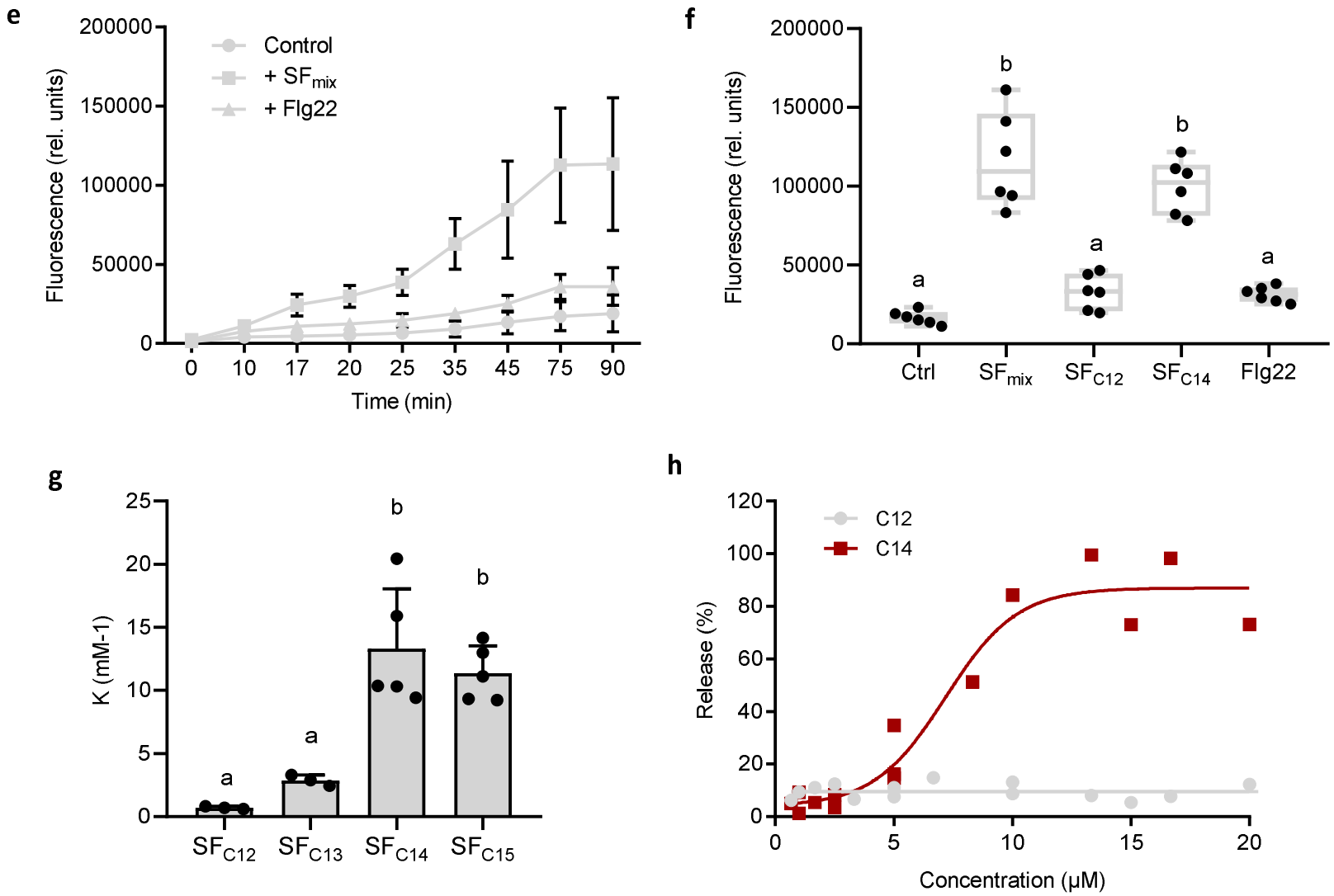
e
Fluorescence (rel. units)
200000
150000
100000
50000
0
Control
+ SFmix
+ Flg22
0
10
17
20
25
35
45
75
90
Time (min)
f
Fluorescence (rel. units)
200000
150000
100000
50000
0
a
b
a
b
a
Ctrl
SFmix
SFC12
SFC14
Flg22
g
K (mM-1)
25
20
15
10
5
0
a
a
b
b
SFC12
SFC13
SFC14
SFC15
h
Release (%)
120
100
80
60
40
20
0
C12
C14
0
5
10
15
20
Concentration (µM)

i

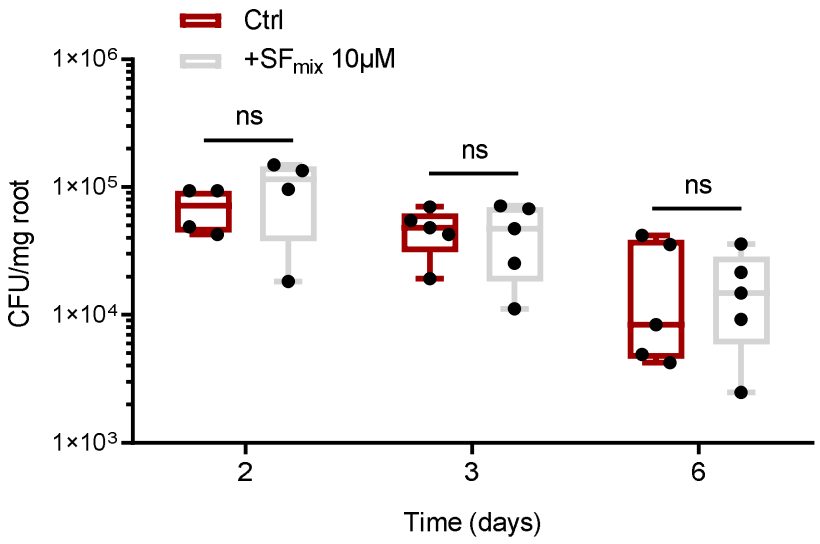
Ctrl
+SF$_{mix}$ 10μM
1×10^6
1×10^5
1×10^4
1×10^3
CFU/mg root
ns
ns
ns
2
3
6
Time (days)

Figure 6: Impact of surfactin homologues on Solanaceae plant immunity. abc Systemic resistance induced in hydroponically-grown tobacco by surfactin and expressed as reduction of *B. cinerea* infection (illustration of the reduction in the diameter of spreading lesions on infected leaves) in plants treated at the root level prior to pathogen inoculation on leaves compared to control plants. Data represent results grouped from two independent experiments with similar results and each involving 5 plants with 4 lesions on the second leave (n=40). **a** Effect of surfactin homologues (SF mix) as naturally co-produced by the bacterium (C12/C13/C14/C15 in relative proportions 8/17/33/42%) **** P-value <0.0001 **b** Effect of HPLC-purified surfactin homologues applied at 10 µM with fatty acid chains from C12 to C15. Significate difference between each condition is indicated by different letters, p-value < 0.05 **c** Effect of the most active C14 homologue tested at various concentrations. Significate difference between each condition is indicated by different letters, p-value < 0.05 **de** Stimulation of oxidative burst in root tissues upon treatment with a SF mix and to the response observed by treating roots with flagellin (flg22, 1 µM) used as positive control. **d** Stimulation of apoplastic ROS accumulation (DCFH-DA fluorescent probe) in root tissues upon treatment with a surfactin mix applied at 15 µM. Means and standard deviations are shown for one representative experiment performed on nine samples per treatment each containing three root segments (approx 100 mg FW) collected from different plants (n=9). Similar trend was obtained in an independent assay. **e** Stimulation of cytoplasmic hydrogen peroxide production in root cells. Means and s.d. were calculated from measurements performed on three samples per treatment each containing three root segments (approx 100 mg FW) collected from different plants. Data represent values obtained from two independent experiments (n=6 per treatment). **f** Stimulation of cytoplasmic hydrogen peroxide production in root cells after treatment with C_{12} and C_{14} surfactin homologues as representative of short and long fatty acid chains respectively. Flg22 as used as control. Significate difference between each condition is indicated by different letters, p-value < 0.0001. **g** Binding coefficient (K) of Surfactin homologues (C_{12} to C_{15}) to large unilamellar vesicles (LUV) composed by PLPC/Sitosterol/Glucosylceramide (60:20:20 molar ratio). Means ± std err. from three to five biological replicates of one representative experiment are shown Significate difference between each condition is indicated by different letters, p-value < 0.05 **h** Release of 8-hydroxypyrene-1,3,6 trisulfonic acid (HPTS) from PLPC/Sitosterol/Glucosylceramide (60:20:20 molar ratio) LUV, upon addition of surfactin C_{12} or C_{14} at different concentrations. The ordinate shows the amount of HPTS released after 15 min in the presence of the C_{12} or C_{14} as a percentage of the total amount released by Triton X-100. **i** Influence of roots pretreatment with 10µM of surfactin (blue boxes) compared to non-treated roots (red boxes) on *B. velezensis* GA1 root colonization. Means ± std err. from five biological replicates of one representative experiment are shown. Ns= non significate.